Structure of the Extracellular Domain of Matrix Protein 2 of Influenza A Virus in Complex with a Protective Monoclonal Antibody

Ki Joon Cho,[a,b,c] Bert Schepens, [b,c] Jong Hyeon Seok,[a] Sella Kim,[a] Kenny Roose,[b,c] Ji-Hye Lee,[a] Rodrigo Gallardo,[d,e] Evelien Van Hamme, [b,c] Joost Schymkowitz,[d,e] Frederic Rousseau,[d,e] Walter Fiers,[b,c] Xavier Saelens,[b,c#] Kyung Hyun Kim[a#]

Department of Biotechnology & Bioinformatics, College of Science & Technology, Korea University, Sejong 339-700, Korea[a]; Inflammation Research Center, VIB, 9052 Ghent, Belgium[b]; Department of Biomedical Molecular Biology, Ghent University, 9052 Ghent, Belgium[c]; Switch Laboratory, VIB. 3000 Leuven, Belgium[d]; Switch Laboratory, Department of Cellular and Molecular Medicine, KULeuven, 3000 Leuven, Belgium[e]

Running Head: Interaction of influenza A M2e and monoclonal antibody

#Address correspondence to Kyung Hyun Kim, khkim@korea.ac.kr or Xavier Saelens, xavier.saelens@irc.vib-ugent.be.

Abstract: 123 words

Main text: 5586 words

ABSTRACT

The extracellular domain of influenza A virus matrix protein 2 (M2, M2e) is conserved and is being evaluated as a quasi-universal influenza A vaccine candidate. We describe the crystal structure at 1.6 Å resolution of M2e in complex with the Fab fragment of an M2e-specific monoclonal antibody that protects against influenza A virus challenge. This antibody binds M2 expressed on the surface of cells infected with influenza A virus. Five out of six complementary determining regions interact with M2e, and three highly conserved M2e residues are critical for this interaction. In this complex, M2e adopts a compact U-shaped conformation stabilized in the centre by the highly conserved tryptophan residue in M2e. This is the first description of the three dimensional structure of M2e.

IMPORTANCE

M2e of influenza A is under investigation as a universal influenza A vaccine, but its three dimensional structure is unknown. We describe the structure of M2e stabilized with an M2e-specific monoclonal antibody that recognizes natural M2. We found that the conserved tryptophan is positioned in the centre of the U-shaped structure of M2e and stabilizes its conformation. The structure also explains why previously reported in vivo escape viruses, selected with a similar monoclonal antibody, carried proline residue substitutions at position 10 in M2.

INTRODUCTION

Matrix protein 2 (M2) is a structural protein of influenza A viruses and plays an important role in the virus life cycle. This long type III membrane protein of 96 amino acid residues has an N-terminal ectodomain (M2e) of 23 residues, a transmembrane domain of 19 residues, and a cytoplasmic domain of 54 residues (1). M2 is classified as a viroporin. Mutational analysis and crystal and NMR structural analysis of the M2 transmembrane domain revealed that it is composed of a four-stranded coiled coil and that two conserved amino acid residues (M2-His37 and -Trp41) have a key role in acid-induced proton gating (2-5). Following endocytosis of influenza A virions, the acidic endosomal environment activates the M2-channel so that protons enter the virion interior. The resulting acidification loosens the viral ribonucleoprotein complexes from matrix protein 1 (M1), which facilitates their migration through the membrane fusion pore into the host cell cytoplasm (6, 7). M2 can activate the inflammasome, impairs autophagosome maturation and was recently shown to recruit parts of the autophagosome machinery to sites of virus budding by a conserved motif in its cytoplasmic domain (8, 9).

The sequence of M2e is conserved and therefore has frequently been explored for the development of a universal influenza A vaccine (10-13). Immune protection by M2e-directed vaccines has been documented extensively in experimental animal models, including mice, ferrets and swine (11-13). In addition, a phase I clinical study showed that M2e-based vaccines are safe and immunogenic in human (10, 14). Seasonal influenza A virus infection induces a poor immune responses to M2e, but this weak response against M2e in humans was boosted following infection with 2009 pandemic H1N1 influenza virus (15). Protection induced by M2e-based vaccines such as M2e displayed on recombinant virus-like particles is mediated by antibodies (11) and, like the *in vitro* broadly neutralizing

HA stalk-specific antibodies (16), depends on activating Fcγ receptors (11, 16, 17). In line with this, passive transfer of mouse and human monoclonal antibodies directed against M2e can protect against influenza A virus challenge (11, 18-21). It has also been reported that treatment of experimentally challenged human volunteers with a human monoclonal antibody directed against M2e reduces viral replication and clinical symptoms (Ramos, E., Options for the Control of Influenza VIII, September 9, 2013)(22).

Crystal structures of the extracellular domain of influenza hemagglutinin (HA) and neuraminidase (NA), either as a free form or as a complex with an Fab or with single chain Fv fragments of monoclonal antibodies, have been described (23). Atomic resolution structures of the M2 transmembrane domain and of part of the cytosolic domain of M2 have also been reported (5). The transmembrane domain forms a four-helix bundle with a helical tilt of approximately 30° relative to the central axis of the bundle. The membrane proximal cytosolic part of M2 forms an amphipathic α helix almost perpendicular to the membrane spanning α helix of M2 (24, 25). However, the three dimensional structure of M2e has remained unknown. Here, we report a high resolution crystal structure of M2e in complex with the Fab of a protective M2e-specific monoclonal antibody (mAb). In this complex, M2e adopts a U-shape with M2-Trp15 positioned in the center. The structure reveals a critical role for M2-Glu6, -Pro10, -Ile11, and -Trp15 in monoclonal antibody binding. This observation explains why previously reported escape viruses, isolated from infected SCID mice treated with a similar M2e-specific mAb, encoded M2 with a Pro10-to-Leu or Pro10-to-His mutation (26).

MATERIALS AND METHODS

Digestion and purification of mAb 65 Fab fragments. Monoclonal antibody 65 (mAb65) is a mouse IgG2a antibody isolated using conventional hybridoma technology and splenocytes from BALB/c mice immunized with M2e-tGCN4 (27). MAb-65 (3 mg) was treated with papain at a ratio of 1:50 (w/w) for 3 h in PBS buffer with 5 mM L-cysteine and 5 mM EDTA at 37ºC. Proteolysis was halted by adding crystalline iodoacetamide to a final concentration of 30 mM. The mixture was then dialyzed against PBS buffer, and the mAb65 antigen-binding fragments (Fab65) was separated from the Fc fragment on a Protein A column. The unbound fraction was further purified by Superdex 200 HR size-exclusion chromatography.

Protein crystallization and data collection. An HPLC-purified synthetic M2e peptide (MSLLTEVETPIRNEWGCRCNDSS, Anygen, Jeollanam-do, Korea) was mixed with purified Fab65 at a 5:1 molar ratio in 20 mM Tris-HCl (pH8.0) and 50 mM NaCl buffer. After 12 h at 4°C, the mixture was loaded two successive times on a Superdex 75 HR column to purify M2e–Fab65 complexes. The complex of M2e peptide with Fab65 in 20 mM Tris-HCl (pH8.0), 50 mM NaCl, and 5 mM DTT was screened for crystal formation by a vapor diffusion method using commercial screening kits and an Oryx4 crystallization robot (Douglas Instruments Ltd., Berkshire, UK). Thin rhombic crystals of M2e–Fab65 complex were obtained in 20% PEG 3350 and 200 mM NaCl in one week. Diffraction data at 1.6 Å resolution of the M2e–Fab65 complex were collected at 100K in a stream of liquid N_2 using synchrotron sources at beamline BL-17A in the Photon Factory (Tsukuba, Japan). For the M2e–Fab65 complex, the space group is P1. All data were processed and scaled using the HKL2000 program (28).

Structure solution and refinement. The heavy chain structure in the M2e–Fab65 complex was solved by molecular replacement (MR) using the heavy chain of Fab CR6261 (PDB ID: 3GBM) as template, and the light chain structure of Fab65 was solved using the light chain of Fab CR6261 after fixing the MR solution of the heavy chain of Fab65. MR was performed by Molrep in CCP4 Suit (29). The initial solution was optimized by rigid body refinement, and correct sequences of Fab65 were applied. Manual adjustment of M2e peptide and Fab65 was conducted in Coot (30) based on difference Fourier maps (2|Fo|-|Fc| and |Fo|-|Fc|) and refinements were carried out using Refmac5 (29). After a few rounds of model rebuilding, water molecules were added at the |Fo|-|Fc| map peaks above 3.0σ. Data and refinement statistics are summarized in Table 1. Prediction of free energy differences of the M2e–Fab65 interface was performed by YASARA at pH7 and 298K (31). The shape complementarity score was calculated using SC in CCP4 Suite. All structural images were created using PyMol (Delano Scientific, http://www.pymol.org).

Biochemical characterization. For peptide ELISA, wild type M2e (SLLTEVETPIRNEWGCRCNDSSDSG), M2eP10L (SLLTEVETLIRNEWGCRCNDSSDSG), or M2eW15G (SLLTEVETPIRNEGGCRCNDSSDSG) were coated on a 96-well Maxisorp plate at 37ºC overnight, followed by blocking with 3% skim milk in PBS buffer. The plate was then incubated with mAb65 or mAb148 (a mouse monoclonal IgG1 antibody that recognizes the first 9 amino acids of M2e) as primary antibodies. After vigorous washing with 0.1% Tween 20 in PBS buffer, binding was detected using HRP-conjugated anti-mouse Abs. For cell-based ELISA, pDWPI-M2-Flag plasmids with the respective alanine mutation were transfected into HEK293T cells using calcium phosphate precipitation. After 24 h, cells were

fixed with 4% paraformaldehyde, and M2e expressed on the cell surface was detected in the same way as the peptide ELISA described above.

For Fourier transform infrared spectroscopy (FTIR), the M2e peptide was dissolved in PBS buffer at 2–4 mg/ml, and FTIR spectra were recorded on a Tensor 27 FT-IR (Bruker Optics GmbH, Ettlingen, Germany) using a Bio-ATRCell II (Harrick Scientific Products Inc., Pleasantville, NY 10570, USA) at 25ºC. The data shown in Fig. 5C are the average of 256 spectra at a resolution of 2 nm.

For alanine-scanning, pDWPI-M2-Flag plasmids with the respective alanine mutation were transfected into HEK293T cells using calcium phosphate precipitation. After 48 h, the cells were lysed in 50 mM Tris-HCl (pH8.0), 150 mM NaCl, 1% NP40, 5 mM EDTA, and proteinase inhibitor cocktail. The lysate was analyzed by western blot using mAb65, mAb 14C2 (Enzo Life Sciences) and anti-Flag antibody (Sigma-Aldrich) as primary antibodies and HRP-conjugated anti-mouse antibody as secondary antibody.

Influenza A virus plaque reduction assay. PR8, WSN, A/USSR/77 and X31 (H3N2) viruses were produced in MDCK cells. An amount of virus corresponding to a predetermined titer of 5~10 PFU/well (of a 96 well microtiter plate) was mixed with 10 fold serial dilution of mAb65 (starting concentration of 10 µg/ml), mAb3G8 (an IgG2a monoclonal antibody specific for Respiratory Syncytial virus small hydrophobic protein), amantadine (starting concentration 100 µM, Sigma) or polyclonal goat anti-PR8 immune serum (NIH Biodefense and Emerging Infections Research Resources Repository NR-3148). After one h incubation at RT, the mixture was transferred to monolayers of MDCK cells seeded in 96-well plates and the plates were incubated at 37ºC. After 1 h, the medium was removed and 0.6% Avicel in serum-free medium containing 1 µg/ml trypsin and antibodies or amantadine was applied as an overlay. Twenty h later, the overlay was removed, cells

were fixed with 4% paraformaldehyde and the plaques were stained with goat anti-RNP antibody (NIH Biodefense and Emerging Infections Research Resources Repository NR-3133), followed by incubation with HRP-labelled donkey anti-goat Ig serum (Santa Cruz Biotechnology Inc., TX, USA) and finally revealed by staining with True-Blue peroxidase substrate (Kirkegaard & Perry Laboratories, Inc, Gaithersburg, MD, USA).

Immunofluorescence microscopy. MDCK cells were seeded at 30,000 cells on glass cover slips in 24-well plates. After 24 h, cells were infected with PR8, pandemic H1N1 2009, Mallard Duck/ALB/1979 (H3N6), Chicken/Nanchang/2001 (H3N2) or Swine/Ontario/2001 (H3N3) (MOI = 0.5), or were mock infected. After 24 h, the cells were fixed with 2% paraformaldehyde in PBS for 30 min on ice. The cells were stained with anti-NP antibody (obtained from BEI Resources, NIAID, NIH: Polyclonal Anti-Influenza Virus RNP, A/Scotland/840/1974 (H3N2), goat antiserum), and mAb148 or mAb65. Images were recorded with a confocal microscope (Leica Sp5 AOBS confocal system).

Reverse genetic virus production. Site-directed mutagenesis of M2e in pHW197-M (32) was performed by polymerase chain reaction (PCR) using primers incorporating the desired mutant sequences. Influenza A virus rescue from the PR/8 plasmid system was performed on a HEK293T-MDCK co-culture as previously described (32). To analyze the expression of M1 and M2, the pHW197-M wild type and mutant plasmids were transfected into HEK293T cells together with pCAXL-PA, pCAXL-PB1, pCAXL-PB2, and pCAXL-NP (33) in 12-well plates. After 48 h, expression was analyzed by western blot using polyclonal goat anti-influenza virus RNP (NIH Biodefense and Emerging Infections Research Resources Repository NR-3133), mAb148, mAb65 and goat anti-M1 antibody as primary antibodies. To generate reverse genetic viruses, pHW193-PA, pHW192-PB1, pHW191-PB2, pHW195-NP, pHW198-NS1, pHW196-NA, pHW194-HA, and mutated pHW197-M were co-

transfected into HEK293T cells and MDCK co-cultures in 6-well plates. After 24 h, 2 µg/ml of trypsin was added to the media, and virus production was assessed by determining hemagglutination activity and plaque forming units in the supernatant. For plaque assay, MDCK cells in a 24-well plate were incubated with virus in serum free-medium at 37ºC. After 1 h, the medium was removed and 0.6% of Avicel in serum-free media containing 2 µg/ml trypsin was used as an overlay. After 2 days at 37ºC, plaques were stained with goat anti-RNP antibody, followed by detection with True-Blue peroxidase substrate (Kirkegaard & Perry Laboratories, Inc, Gaithersburg, MD, USA).

Protein structure accession number. The M2e peptide and Fab65 complex structure has been deposited in the Protein Data Bank (PDB) under the PDB code 4N8C.

RESULTS

Structure of M2e in complex with monoclonal antibody 65. We isolated a monoclonal antibody (mAb65, IgG2a) from BALB/c mice that had been immunized with a soluble tetrameric form of M2e (M2e-tGCN4) (27). Passive transfer of mAb65 protected laboratory mice against influenza A virus challenge (34). First, we crystallized M2e-tGCN4 but were unable to accurately model the M2e part because its electron density map was too weak (data not shown). We then crystallized an M2e-peptide comprising amino acids 1–23 complexed with Fab65. The crystals diffracted X-rays to 1.6 Å resolution and allowed us to model the heavy chain (H) from residues 1 to 221, the light chain (L) from residues 1 to 220 of mAb65, and M2e from residues 2 to 16 (Fig. 1A). This structure showed that all three heavy chain CDRs (HCDRs) and light chain CDRs (LCDRs) 1 and 3 contact M2e (Fig. 1B). The total surface area of the peptide that is buried by the Fab is 747.9 $Å^2$ and that of the Fab buried by M2e is 655.6 $Å^2$, which are larger than those reported for the complex between motavizumab and a human respiratory syncytial virus F-derived peptide (35). The shape complementarity score of the M2e–Fab65 interface is high (0.77 for HCDRs and 0.90 for LCDRs), exceeding that of HA stem-Fab complexes (Fig. 1C).

The interactions between M2e and Fab65 CDRs are mainly through His35, Asn55, Asn59 and Arg99 of the HCDRs, and the hydroxyl groups of Tyr31, Tyr98 and Tyr100 in the LCDRs. M2-Glu6 is a key interacting residue. Its side chain carboxyl group forms a salt bridge with the side chains of His35 (HCDR1) and Arg99 (HCDR3) as well as a hydrogen bond with the main chain nitrogen of Ala33 in HCDR1 (Fig. 2A). M2-Glu6 also interacts with the main chain oxygen of Ala33 and the main chain nitrogen of Arg99 in HCDR3 through a water molecule (Fig. 2A). The main chain oxygen of M2-Glu6 also forms a hydrogen bond with the hydroxyl group of Tyr100 of LCDR3. Moreover, M2-Glu6 is

218 associated with residues Thr30, Tyr32, Ala33, Thr53 and Asp54 in the HCDRs via water-
219 mediated hydrogen-bond networks (Fig. 2B). It is known that water molecules can form an
220 intricate network that makes antibody-antigen interfaces fully complementary (36, 37).
221 Additionally, the side chain of M2-Glu8 interacts with those of Asn55 and Asn57 of the
222 HCDR2 through water molecules, and its main chain oxygen interacts with the main chain
223 nitrogen of Tyr100 of LCDR3, again through a water molecule (Fig. 2B). The carboxyl
224 group of M2-Glu14 interacts directly with the hydroxyl group of Tyr31 of LCDR1 and
225 Tyr98 of LCDR3 through a hydrogen-bond network (Fig. 2B). The main chains of M2-Val7,
226 -Pro10, -Arg12 and -Asn13 and the side chains of M2-Thr5, -Arg12, and -Asn13 also
227 facilitate hydrophilic interactions with different residues in the CDRs (Fig. 2C). Finally, a
228 hydrophobic patch formed by M2-Pro10 and -Ile11 occupies a hydrophobic pocket formed
229 by residues Val104 of HCDR3 and Tyr31, Tyr34, Leu38, Tyr98, Tyr100 and Leu102 of
230 LCDR1 and LCDR3 (Fig. 2D).

231 **M2-Pro10 and M2-Ile11 are essential for recognition by mAb65.** Although the first 9
232 amino acid residues of M2e are strongly conserved, starting from position 10 there is
233 considerable variation. This is likely because this part of M2 overlaps with the C-terminal
234 part of M1 in a +1 translational frame shift. Assuming a stronger selection pressure on M1,
235 this implies that single nucleotide alterations at the wobble position in the M1 codons can be
236 tolerated and result in amino acid alterations in that part of M2e. Still, we noted that M2-
237 Trp15 and to a slightly lesser extent the cysteine residues at positions 17 and 19 in M2 are
238 nearly absolutely conserved in all available M2 sequences of influenza A viruses. To better
239 understand the relative contribution of the M2e residues for mAb65 binding, we first
240 performed an Ala-scan mutagenesis of M2e. For this we used M2 fused at its C-terminus
241 with a Flag tag to allow normalization of expression levels, and cloned the corresponding

coding information in a mammalian expression vector. This Ala-scan analysis revealed that the epitope-specificity of mAb65 is similar to that of monoclonal antibody 14C2 (Fig. 2E) (38). In addition, we found that M2 amino acids Glu6, Pro10, Ile11 and Trp15 are critical for mAb65 and, to a lesser extent, also Thr5 and Glu14 (Fig. 2E). It was surprising that M2-Trp15 was crucial for mAb 65 binding, because based on our crystal structure it did not make any direct contact with mAb65.

Next, we immunostained cells pre-infected with different subtypes of influenza A viruses differing in their M2e sequences. MAb65 recognized M2 on the surface of cells infected with A/Puerto Rico/8/1934 virus (PR8) but bound poorly to M2 expressed by pandemic H1N1 2009, avian, and swine influenza viruses (Fig. 3A and 3B). This confirms the importance of Pro10 and Ile11 for mAb65 binding and is in line with the structural data. Indeed substitution of M2-Pro10 by His (as in Chicken/Nanchang/2001) would replace a hydrophobic residue with a polar one and reduce interactions with the hydrophobic patch at the bottom of the Fab65 paratope. In addition, the side chains of His and Leu (as in Mallard Duck/ALB/1979) would result in a steric clash, whereas an Ala residue at this position would be poorly hydrophobic. Likewise, replacement of M2-Ile11 by Thr (as in 2009 pH1N1 and the avian and swine influenza viruses tested here) would replace a hydrophobic residue by a polar one, and substitution by Ala would contribute too little hydrophobicity to allow proper binding in the hydrophobic part of the Fab65 paratope.

It has been reported that some influenza A virus strains display a reduced plaque size phenotype when grown in the presence of 14C2 monoclonal antibody (39). Since mAb65 and 14C2 react very similar in the Ala-scan mutagenesis, suggesting a comparable epitope in M2e, we evaluated the potency of mAb65 to inhibit virus growth in a plaque assay. Growth of these four viruses (PR8, WSN, A/USSR/77 and X31) in the presence of mAb65 did not

result in less or smaller plaques, whereas amantadine and convalescent serum from infected mice, reduced plaque numbers (Fig. 3C).

We further investigated the importance of M2-Pro10 for Fab65 binding by peptide and cell ELISA. mAb65 readily bound to M2e peptide or cells expressing WT M2. Notably, substitution of M2-Pro10 to Ala or Leu strongly reduced binding of mAb65 but had only a minor effect on mAb148 (Fig. 4A and 4B).

M2-Trp15 stabilizes the M2e conformation. In the Fab65 complex, M2e adopts a remarkably compact structure with a β-turn from Thr5 to Glu8 and a 3_{10}-helix from Ile11 to Trp15 (Fig. 5A). Due to the distinct U-shape, M2e-Leu4 and M2e-Gly16 are only 3.1 Å apart (Fig. 5A). This compact conformation of M2e is maintained by intra-molecular hydrophilic and hydrophobic interactions. The key residue in these intra-molecular interactions is M2e-Trp15 (Fig. 5A). Hydrophobic interactions are formed between the indole ring of M2e-Trp15 and the aliphatic parts of M2e-Glu6 and M2e-Arg12. The central position of M2e-Trp15 in M2e resembles the positioning of tryptophan in so-called Trp-cages, which fold into stable mini-proteins (40). As in Trp-cages, the indole ring nitrogen of M2e-Trp15 hydrogen-bonds with the carbonyl oxygen of M2e-Thr9, and a network of other hydrogen bonds between main chain carbonyl oxygens and nitrogens of M2e confines M2e-Trp15 in a central position (Fig. 5A and 5B). For such variant peptides in complex with Fab65, the predicted free energy score of M2e in which Trp15 is replaced by other amino acids strongly increases (2.39-6.48 kcal/mol).

To identify structural patterns in M2e peptide in solution that could correspond to those observed in the crystal structure of the Fab65–M2e complex, we analyzed wild type M2e, M2eP10L and M2eW15G peptides by Fourier transform infrared spectroscopy (FTIR). This analysis revealed absorbance peaks and frequencies of amide I, indicating that all peptides

290 contain an α-helical component (peak near 1650 cm^{-1}, Fig. 5C). Wild type M2e and
291 M2eW15G peptides also displayed a pronounced β-turn component (peaks from 1669 to
292 1683 cm^{-1}), possibly corresponding to the β-turn in the crystal structure. The FTIR spectrum
293 of M2eP10L differed substantially from that of wild type and M2eW15G peptides, and
294 showed characteristics of β-sheets (split peak at 1692 and 1615 cm^{-1}, Fig. 5C) (41). The
295 absence of a β-turn further helps to explain loss of binding of mAb65 to M2e with Pro10
296 substitutions and was confirmed in a peptide ELISA (Fig. 4A).
297 When Trp15 was replaced by Gly, binding of mAb65 to M2e peptide in ELISA was strongly
298 reduced (Fig. 4A and 4B). The crucial position of Trp15 in the M2e three-dimensional
299 structure together with its near absolute sequence conservation in influenza A viruses,
300 including bat H17N10 and H18N11 viruses, is intriguing. At the genetic level, it is
301 impossible to substitute any nucleotide in M2-Trp15 without altering Met244 or Gly245 in
302 M1 (Fig. 6A). Therefore, its conservation might be imposed by a critical role of the
303 overlapping codons in M1. Nevertheless, we introduced several substitutions for Trp15 in
304 M2 and tried to rescue influenza A virus using an eight plasmid-based reverse genetics
305 system for PR8 virus (32). All M2e variant viruses that we attempted to obtain would
306 express mutant M1 except for the M2-STOP virus, in which a stop codon is introduced after
307 M2-Asp24. Mutations M2-Trp15Ala, -Trp15Arg, -Trp15Gly and -Trp15Leu resulted in
308 substitution of methionine at position 244 in M1 into Ser, Thr, Arg and Thr, respectively.
309 Replacement of M2-Trp15 by Cys resulted in substitution of Gly into Arg at position 245 in
310 M1. When we transfected the eight plasmid, we found that M1 and M2 expression levels
311 were comparable for all mutants except M2-STOP, indicating that the introduced mutations
312 did not affect the stability of these proteins (Fig. 6B). However, we could only rescue viruses
313 derived from the M2-Trp15Cys and M2-STOP constructs, but the number of plaques were

very low (Fig. 6C and 6D). We tried several times to rescue virus from the plasmid combinations in which M2-Trp15 was changed into Ala, Arg, Gly or Leu (and M1 at position 244) without success. Although we cannot exclude that this result may be due to technical failure, this outcome suggests that M2-Trp15 and or M1-Met244 play an important role in virus replication. We did obtain virus from the M1-Gly245Arg/M2-Trp15Cys mutant plasmid but this virus replicated poorly as evidenced by the small plaque size and low virus titer (Fig 6C). Taken together, M2-Met244 and/or M2-Trp15 possibly play an important role in the virus life cycle.

DISCUSSION

We describe the crystal structure of a prototypical M2e peptide in complex with a mouse monoclonal antibody. To our knowledge, this is the first report of a three dimensional structure of M2e. Our findings help to complete our knowledge of the atomic resolution structure of the domains of influenza A proteins that face the outside of virions and of infected cells. To determine this structure, we used a monoclonal antibody that had been isolated following immunization of BALB/c mice with M2e-tGCN4, a soluble tetrameric M2e immunogen, which we considered a good mimic of M2e in natural M2 (27). Furthermore, this monoclonal antibody protects laboratory mice against challenge with PR/8 virus, and its specificity is similar to that of mAb 14C2, first described by Zebedee and Lamb (39) (Fig. 2E).

We first tried to resolve the structure of M2e-tGCN4 crystals. This structure revealed that the leucine-zipper part of M2e-tGCN4 makes an angle of 15° relative to the four-fold symmetry axis (data not shown). Unfortunately, we could not accurately model the M2e part of M2e-tGCN4 because the electron density map was too weak, possibly due to the high flexibility of M2e. Therefore, we decided to stabilize the M2e peptide with Fab65. An important question is the extent to which this structure resembles natural M2e as it exists in virions and on the surface of infected cells. It is likely that natural M2e is flexible and that the structure we propose here is a snapshot of one of several conformations that M2e can adopt. However, several lines of evidence support the notion that the structure of M2e in complex with Fab65 does not represent merely a rare and very transient M2e conformation. First, next to binding to the M2e-tGCN4 immunogen used for the generation of Mab65, this monoclonal antibody binds with high specificity to the M2 ectodomain on the surface of infected or transfected cells and to M2 in Western blots. The binding of mAb65 to infected cells or to M2 (analyzed

by Western blot) depends on the M2e amino acids involved in the interaction between Fab65 and M2e as observed in the crystal structure. Moreover, administration of low amounts of mAb65 protects mice against influenza A virus challenge. Hence, the M2e conformation we describe does occur at biologically relevant levels on the surface of infected cells. Second, the affinity (Kd = 0.4 nM), Kon (2.24 x 10^5 $M^{-1}.s^{-1}$) and Koff (9.2.10^5 x s^{-1}) of mAb65 for M2e (Van den Hoecke et al., in preparation) are high and in the range that is known to be required for specific antibody–protein interactions (42). Finally, the well-known M2e-specific mAb 14C2 generated by immunization with SDS-PAGE purified M2 binds to the same epitope as Mab65 (Fig. 2E). Together, these observations suggest that the structure of M2e in complex with Fab65 represents of that of non-complexed M2e at the surface of infected cells.

MAb65 bound to M2 on the surface of cells infected with PR/8 virus but not to cells infected with influenza A viruses expressing M2 with a Pro10 and or Ile11 substitution, such as pandemic H1N1 2009 or the avian influenza viruses that we tested. The importance of these two residues for Fab65 binding was clear from the crystal structure: M2e-Pro10 and -Ile11 form a hydrophobic patch that neatly fits into a hydrophobic pocket consisting of Val104 in HCDR3 and Tyr31, Tyr34, Leu38, Tyr98, Tyr100 and Leu102 in LCDR1 and LCDR 3. mAb65, like 14C2, has a LCDR1 loop 17 amino acids long. This loop completely covers the hydrophobic patch of M2e peptide (Fig. 1A). The involvement of M2e-Pro10 and -Ile11 in the interaction with the paratope is consistent with the Ala-scan results and YASARA-based predictions with FoldX plug-in (31): a Pro-to-Ala change would result in a loss of 2.16 kcal/mol of interaction energy, and an Ile-to-Ala change at position 11 in a loss of 3.48 kcal/mol. Generally, amino acid residues that contribute more than 2.5 kcal/mol of free

energy difference in a protein–protein interaction interface are essential for specificity and stability of the interaction (43).

More than 90% of the publicly available influenza A M2 sequences have Pro10, and most of the replacements are Pro10His and Pro10Leu. In particular, many human H1N1 viruses with M2-His10 have emerged. In human influenza strains, M2-Leu10 was mainly observed among humans infected with avian influenza virus (H5N1, H9N2, and more recently H7N9). A crucial role of Pro10 for the interaction of mAbs with M2e was also apparent from a previous study showing that P10H and P10L PR/8 escape virus mutants arose in SCID mice in the presence of 14C2-like anti-M2e mAbs (26). When modeled in the structure of M2e, these mutations induce steric hindrance at the interfaces with LCDR3 and HCDR3, explaining the reduced binding and the selective advantage of escape viruses with M2-Pro10 substitutions under M2e-specific mAb selection pressure. M2-Ile11 is highly conserved in human H1N1 viruses that circulated until 2009 (> 96% prevalence), but it changed to Thr11 in the 2009 pandemic H1N1 virus. Substitution of M2e-Ile11 to Thr11 reduces the possibilities for hydrophobic interactions with Tyr31, Tyr34, Leu38 and Tyr98 in the L-chain, and YASARA plot analysis indicated a significant energy change of 2.6 kcal/mol. This explains why the binding of mAb65 to M2 of the 2009 pandemic H1N1 is weak (Fig. 3). M2-Glu6, -Glu8, and -Glu14 are responsible for most of the hydrophilic interactions with mAb65. The side chain of M2e-Glu6 contributes four hydrophilic interactions with Fab65, either directly or via water molecules. According to YASARA, mutation of M2-Glu6 to Ala would disrupt most of these hydrogen bonded interactions and result in a predicted free energy difference of 3.44 kcal/mol at the M2e–Fab65 interface. Given the importance of M2-Glu6 for binding with Fab65, an escape virus with an M2-Glu6 substitution would most likely not be controlled by mAb65-like antibodies. However, this would imply an amino acid

substitution in M1 and M2, and as M1 is among the most conserved proteins of influenza A, such a mutation may generate an unfit virus.

Recently, solid-state NMR of full-length, lipid-embedded M2 revealed that the secondary structure of M2e changed with membrane composition (44). DMPC (1,2-dimyristoyl-sn-glycero-3-phosphocholine)-bound M2 exhibited a β-sheet conformation and was highly dynamic, whereas M2 bound to cholesterol-containing membranes had a predominantly α-helical conformation. The N-terminal residues SLLTEVET are identical in M1 and M2, and this sequence forms an α-helix in M1 (45). FTIR analysis of M2e peptide suggests that M2e has α-helical and β-turn conformations in solution, and a β-turn is present in the M2e-Fab complex structure. The antibody recognition motif in a peptide is often a β-turn, and antigenic peptides have a tendency to adopt β-turns in solution (46-48). Additionally, peptide antigens that stabilize a β-turn have been shown to increase antibody affinity (46, 49). Having a stable conformation with a β-turn involved in antibody binding resembles that of the N-terminal peptide of HIV-1 Tat bound to a monoclonal antibody (48). We propose that natural M2e temporarily adopts a (curled) shape that is first selected and then becomes fixed upon antibody binding. Such a scenario is in line with the explanation proposed for the specificity of the interactions between ubiquitin and the many different ubiquitin-binding proteins in a cell (50). Ubiquitin-binding proteins selectively bind one particular conformation of ubiquitin from a set of many. However, the relationship between the biological function of M2e and the potential advantages of its structural adaptability remains unclear.

The central position of Trp15 in the M2e structure is remarkable and resembles so-called Trp-cages, which are synthetic miniproteins that fold spontaneously into globular structures, containing a hydrophobic core and a helical segment (51). The comparison of M2e with Trp-

cages suggests that M2-Pro10 might also contribute to the folding of M2 because the rigidity of proline orients the main chain oxygen of M2-Thr9 in a position that allows the formation of hydrophilic interactions with the indole ring of Trp15 (Fig. 5A and 5B)(51). Results of Ala-scan mutagenesis and ELISA indicated an important contribution of M2-Trp15 to mAb65 binding (Fig. 2E and Fig. 4A) even though this residue did not bind to the antibody. The FTIR spectrum of M2eW15G was nearly identical to that of wild type M2e, suggesting that M2-Trp15 controls the tertiary structure but not the secondary structure of M2e (Fig. 5C). M2-Trp15 is extremely conserved: only eight mutations occur at this position in over 28,000 M2 sequence entries in the NCBI databank. M42, which has a different M2e sequence, could functionally replace M2 (52). Even in this case, as well as in the predicted M2 proteins of the H17N10 and H18N11 influenza viruses, M2-Trp15 is conserved (53). We could not rescue M1-Met244/M2-Trp15 mutant viruses. It is possible that failure to rescue these viruses was due to a possible role for M2-Trp15 in the ion channel activity of M2. However, we found that transfection of HEK293T cells with wild type or M2-Trp15 mutant expression vectors, was equally cytotoxic and resulted in a comparable increase in the luminal pH of the Golgi (unpublished results). M2-Trp15 mutant viruses inevitably have M1 mutations, and it cannot be ruled out that the reason for the very high sequence conservation of M2-Trp15 is driven by the functional conservation of Arg243, Met244, and Gly245 of M1. Although the part of M1 following Ala200 does not affect binding to vRNPs (54), it is involved in determining the morphology of influenza A virus (55).

Anti-M2e antibodies generally inhibit viruses not by direct neutralization but by antibody-dependent cell-mediated cytotoxicity and antibody-dependent cell-mediated phagocytosis (17). This is partly related to the small number of M2 proteins that are incorporated in virions (20 to 60 molecules/virion) despite the abundance of M2 on the infected cell surface

(1, 39). Grandea *et al*. reported that human monoclonal antibodies TCN-031 and TCN-032 bind to influenza A virions (19). These two antibodies bind to the N-terminal end (Ser2 to Glu6). Fu *et al*. reported that oligomerization of M2e improves the affinity of M2e-specific antibodies and protection of mice against lethal influenza virus challenge (56). Therefore, despite its small size, it is likely that M2e is dynamic and displays various conformations that can be targeted by different antibodies with different affinities.

In summary, our study reveals, for the first time, a snapshot of the structure of M2e. We propose that M2e has different conformations, including a curled structure that can induce high affinity M2e-specific antibodies. The structure of M2e in complex with a protective antibody may guide the design of an M2e vaccine with a stabilized conformation. According to the structure described here, mutation of Pro10-to-His or Ile11-to-Thr will abolish binding. This implies that circulating influenza viruses with M2-His10 or -Thr11 would not be bound by mAb65-like antibodies. However, active vaccination strategies induce an oligoclonal response to M2e, and some human monoclonal antibodies recognize the N-terminal part of M2e, suggesting that M2e remains a universal influenza A vaccine candidate.

459 **ACKNOWLEDGEMENTS**

460 We thank Liesbeth Vande Ginste, Anouk Smet and Tine Ysenbaert for excellent technical
461 support and Dr. Wim Nerinckx for helpful discussions. We also thank Amanda Goncalves
462 and the other staff of VIB Microscopy core facility for their outstanding support and advice.
463 KJC was supported by the Korean Research Foundation and by FWO project 3G052412N.
464 BS is an FWO-Vlaanderen postdoctoral fellow and KR was supported by SBO grant 110038
465 from IWT-Vlaanderen. This work was supported by grants from Mid-Career Researcher
466 (KHK 2010-0029242), Transgovernmental Enterprise for Pandemic Influenza (TEPIK) and
467 BK21 plus programs through NRF of the ME (Korea), by IUAP BELVIR project p7/45 and
468 Ghent University Special Research Grant BOF12/GOA/014. The Switch Laboratory was
469 supported by grants from VIB, University of Leuven, the Funds for Scientific Research
470 Flanders (FWO), the Flanders Institute for Science and Technology (IWT) and the Federal
471 Office for Scientific Affairs of Belgium (Belspo), IUAP P7/16. We thank Dr. Webster from
472 St. Jude Children's Research Hospital for providing the A/PR/8/34 based eight-plasmid
473 system for generating recombinant influenza A viruses, BEI Resources for providing antisera
474 against influenza A antigens, and the technical support from the staff at beam lines of Photon
475 Factory (BL-17A) synchrotrons.

476

477

REFERENCES

1. **Lamb RA, Zebedee SL, Richardson CD.** 1985. Influenza virus M2 protein is an integral membrane protein expressed on the infected-cell surface. Cell **40:**627-633.
2. **Stouffer AL, Acharya R, Salom D, Levine AS, Di Costanzo L, Soto CS, Tereshko V, Nanda V, Stayrook S, DeGrado WF.** 2008. Structural basis for the function and inhibition of an influenza virus proton channel. Nature **451:**596-599.
3. **Pinto LH, Dieckmann GR, Gandhi CS, Papworth CG, Braman J, Shaughnessy MA, Lear JD, Lamb RA, DeGrado WF.** 1997. A functionally defined model for the M2 proton channel of influenza A virus suggests a mechanism for its ion selectivity. Proceedings of the National Academy of Sciences of the United States of America **94:**11301-11306.
4. **Cady SD, Schmidt-Rohr K, Wang J, Soto CS, Degrado WF, Hong M.** 2010. Structure of the amantadine binding site of influenza M2 proton channels in lipid bilayers. Nature **463:**689-692.
5. **Schnell JR, Chou JJ.** 2008. Structure and mechanism of the M2 proton channel of influenza A virus. Nature **451:**591-595.
6. **Bukrinskaya AG, Vorkunova NK, Pushkarskaya NL.** 1982. Uncoating of a rimantadine-resistant variant of influenza virus in the presence of rimantadine. The Journal of general virology **60:**61-66.
7. **Hay AJ, Wolstenholme AJ, Skehel JJ, Smith MH.** 1985. The molecular basis of the specific anti-influenza action of amantadine. The EMBO journal **4:**3021-3024.
8. **Gannage M, Dormann D, Albrecht R, Dengjel J, Torossi T, Ramer PC, Lee M, Strowig T, Arrey F, Conenello G, Pypaert M, Andersen J, Garcia-Sastre A, Munz C.** 2009. Matrix protein 2 of influenza A virus blocks autophagosome fusion with lysosomes. Cell host & microbe **6:**367-380.
9. **Beale R, Wise H, Stuart A, Ravenhill BJ, Digard P, Randow F.** 2014. A LC3-interacting motif in the influenza A virus M2 protein is required to subvert autophagy and maintain virion stability. Cell host & microbe **15:**239-247.
10. **Schotsaert M, De Filette M, Fiers W, Saelens X.** 2009. Universal M2 ectodomain-based influenza A vaccines: preclinical and clinical developments. Expert review of vaccines **8:**499-508.
11. **Neirynck S, Deroo T, Saelens X, Vanlandschoot P, Jou WM, Fiers W.** 1999. A universal influenza A vaccine based on the extracellular domain of the M2 protein. Nat Med **5:**1157-1163.
12. **Fan J, Liang X, Horton MS, Perry HC, Citron MP, Heidecker GJ, Fu TM, Joyce J, Przysiecki CT, Keller PM, Garsky VM, Ionescu R, Rippeon Y, Shi L, Chastain MA, Condra JH, Davies ME, Liao J, Emini EA, Shiver JW.** 2004. Preclinical study of influenza virus A M2 peptide conjugate vaccines in mice, ferrets, and rhesus monkeys. Vaccine **22:**2993-3003.
13. **Kitikoon P, Vincent AL, Janke BH, Erickson B, Strait EL, Yu S, Gramer MR, Thacker EL.** 2009. Swine influenza matrix 2 (M2) protein contributes to protection against infection with different H1 swine influenza virus (SIV) isolates. Vaccine **28:**523-531.
14. **Turley CB, Rupp RE, Johnson C, Taylor DN, Wolfson J, Tussey L, Kavita U, Stanberry L, Shaw A.** 2011. Safety and immunogenicity of a recombinant M2e-flagellin influenza vaccine (STF2.4xM2e) in healthy adults. Vaccine **29:**5145-5152.

15. **Zhong W, Reed C, Blair PJ, Katz JM, Hancock K, for the Influenza Serology Working G.** 2014. Serum Antibody Response to Matrix Protein 2 Following Natural Infection With 2009 Pandemic Influenza A(H1N1) Virus in Humans. The Journal of infectious diseases.
16. **DiLillo DJ, Tan GS, Palese P, Ravetch JV.** 2014. Broadly neutralizing hemagglutinin stalk-specific antibodies require FcgammaR interactions for protection against influenza virus in vivo. Nat Med **20:**143-151.
17. **El Bakkouri K, Descamps F, De Filette M, Smet A, Festjens E, Birkett A, Van Rooijen N, Verbeek S, Fiers W, Saelens X.** 2011. Universal vaccine based on ectodomain of matrix protein 2 of influenza A: Fc receptors and alveolar macrophages mediate protection. J Immunol **186:**1022-1031.
18. **Beerli RR, Bauer M, Schmitz N, Buser RB, Gwerder M, Muntwiler S, Renner WA, Saudan P, Bachmann MF.** 2009. Prophylactic and therapeutic activity of fully human monoclonal antibodies directed against influenza A M2 protein. Virology journal **6:**224.
19. **Grandea AG, 3rd, Olsen OA, Cox TC, Renshaw M, Hammond PW, Chan-Hui PY, Mitcham JL, Cieplak W, Stewart SM, Grantham ML, Pekosz A, Kiso M, Shinya K, Hatta M, Kawaoka Y, Moyle M.** 2010. Human antibodies reveal a protective epitope that is highly conserved among human and nonhuman influenza A viruses. Proceedings of the National Academy of Sciences of the United States of America **107:**12658-12663.
20. **Treanor JJ, Tierney EL, Zebedee SL, Lamb RA, Murphy BR.** 1990. Passively transferred monoclonal antibody to the M2 protein inhibits influenza A virus replication in mice. Journal of virology **64:**1375-1377.
21. **Wang R, Song A, Levin J, Dennis D, Zhang NJ, Yoshida H, Koriazova L, Madura L, Shapiro L, Matsumoto A, Yoshida H, Mikayama T, Kubo RT, Sarawar S, Cheroutre H, Kato S.** 2008. Therapeutic potential of a fully human monoclonal antibody against influenza A virus M2 protein. Antiviral research **80:**168-177.
22. **Ramos EL, Mitcham JL, Koller TD, Bonavia A, Usner DW, Balaratnam G, Fredlund P, Swiderek KM.** 2014. Efficacy and Safety of Treatment with an Anti-M2e Monoclonal Antibody in Experimental Human Influenza. The Journal of infectious diseases.
23. **Gamblin SJ, Skehel JJ.** 2010. Influenza hemagglutinin and neuraminidase membrane glycoproteins. The Journal of biological chemistry **285:**28403-28409.
24. **Pielak RM, Chou JJ.** 2010. Solution NMR structure of the V27A drug resistant mutant of influenza A M2 channel. Biochemical and biophysical research communications **401:**58-63.
25. **Cross TA, Dong H, Sharma M, Busath DD, Zhou HX.** 2012. M2 protein from influenza A: from multiple structures to biophysical and functional insights. Current opinion in virology **2:**128-133.
26. **Zharikova D, Mozdzanowska K, Feng J, Zhang M, Gerhard W.** 2005. Influenza type A virus escape mutants emerge in vivo in the presence of antibodies to the ectodomain of matrix protein 2. Journal of virology **79:**6644-6654.
27. **De Filette M, Martens W, Roose K, Deroo T, Vervalle F, Bentahir M, Vandekerckhove J, Fiers W, Saelens X.** 2008. An influenza A vaccine based on tetrameric ectodomain of matrix protein 2. The Journal of biological chemistry **283:**11382-11387.

28. **Otwinowski Z, Minor W.** 1997. Processing of X-ray diffraction data collected in oscillation mode. Method Enzymol **276:**307-326.
29. **Winn MD, Ballard CC, Cowtan KD, Dodson EJ, Emsley P, Evans PR, Keegan RM, Krissinel EB, Leslie AG, McCoy A, McNicholas SJ, Murshudov GN, Pannu NS, Potterton EA, Powell HR, Read RJ, Vagin A, Wilson KS.** 2011. Overview of the CCP4 suite and current developments. Acta crystallographica. Section D, Biological crystallography **67:**235-242.
30. **Emsley P, Cowtan K.** 2004. Coot: model-building tools for molecular graphics. Acta crystallographica. Section D, Biological crystallography **60:**2126-2132.
31. **Van Durme J, Delgado J, Stricher F, Serrano L, Schymkowitz J, Rousseau F.** 2011. A graphical interface for the FoldX forcefield. Bioinformatics **27:**1711-1712.
32. **Hoffmann E, Krauss S, Perez D, Webby R, Webster RG.** 2002. Eight-plasmid system for rapid generation of influenza virus vaccines. Vaccine **20:**3165-3170.
33. **Verhelst J, Parthoens E, Schepens B, Fiers W, Saelens X.** 2012. Interferon-inducible protein Mx1 inhibits influenza virus by interfering with functional viral ribonucleoprotein complex assembly. Journal of virology **86:**13445-13455.
34. **De Baets S, Schepens B, Sedeyn K, Schotsaert M, Roose K, Bogaert P, Fiers W, Saelens X.** 2013. Recombinant influenza virus carrying the respiratory syncytial virus (RSV) F85-93 CTL epitope reduces RSV replication in mice. Journal of virology **87:**3314-3323.
35. **McLellan JS, Chen M, Kim A, Yang Y, Graham BS, Kwong PD.** 2010. Structural basis of respiratory syncytial virus neutralization by motavizumab. Nature structural & molecular biology **17:**248-250.
36. **Levy Y, Onuchic JN.** 2004. Water and proteins: a love-hate relationship. Proceedings of the National Academy of Sciences of the United States of America **101:**3325-3326.
37. **Nakasako M.** 2004. Water-protein interactions from high-resolution protein crystallography. Philosophical transactions of the Royal Society of London. Series B, Biological sciences **359:**1191-1204; discussion 1204-1196.
38. **Zhang M, Zharikova D, Mozdzanowska K, Otvos L, Gerhard W.** 2006. Fine specificity and sequence of antibodies directed against the ectodomain of matrix protein 2 of influenza A virus. Molecular immunology **43:**2195-2206.
39. **Zebedee SL, Lamb RA.** 1988. Influenza A virus M2 protein: monoclonal antibody restriction of virus growth and detection of M2 in virions. Journal of virology **62:**2762-2772.
40. **Scian M, Lin JC, Le Trong I, Makhatadze GI, Stenkamp RE, Andersen NH.** 2012. Crystal and NMR structures of a Trp-cage mini-protein benchmark for computational fold prediction. Proceedings of the National Academy of Sciences of the United States of America **109:**12521-12525.
41. **Kong J, Yu S.** 2007. Fourier transform infrared spectroscopic analysis of protein secondary structures. Acta biochimica et biophysica Sinica **39:**549-559.
42. **Caoili SE.** 2012. On the meaning of affinity limits in B-cell epitope prediction for antipeptide antibody-mediated immunity. Advances in bioinformatics **2012:**346765.
43. **Ofran Y, Rost B.** 2007. Protein-protein interaction hotspots carved into sequences. PLoS computational biology **3:**e119.
44. **Liao SY, Fritzsching KJ, Hong M.** 2013. Conformational analysis of the full-length M2 protein of the influenza a virus using solid-state NMR. Protein science : a publication of the Protein Society.

45. **Arzt S, Baudin F, Barge A, Timmins P, Burmeister WP, Ruigrok RW.** 2001. Combined results from solution studies on intact influenza virus M1 protein and from a new crystal form of its N-terminal domain show that M1 is an elongated monomer. Virology **279:**439-446.

46. **Campbell AP, Sykes BD, Norrby E, Assa-Munt N, Dyson HJ.** 1996. Solution conformation of an immunogenic peptide derived from the principal neutralizing determinant of the HIV-2 envelope glycoprotein gp125. Folding & design **1:**157-165.

47. **Molins MA, Contreras MA, Fita I, Pons M.** 1998. Solution conformation of an immunogenic peptide from HRV2: comparison with the conformation found in a complex with a Fab fragment of an anti-HRV2 neutralizing antibody. Journal of peptide science : an official publication of the European Peptide Society **4:**101-110.

48. **Serriere J, Dugua JM, Bossus M, Verrier B, Haser R, Gouet P, Guillon C.** 2011. Fab'-induced folding of antigenic N-terminal peptides from intrinsically disordered HIV-1 Tat revealed by X-ray crystallography. Journal of molecular biology **405:**33-42.

49. **Dyson HJ, Wright PE.** 1995. Antigenic peptides. FASEB journal : official publication of the Federation of American Societies for Experimental Biology **9:**37-42.

50. **Wlodarski T, Zagrovic B.** 2009. Conformational selection and induced fit mechanism underlie specificity in noncovalent interactions with ubiquitin. Proceedings of the National Academy of Sciences of the United States of America **106:**19346-19351.

51. **Neidigh JW, Fesinmeyer RM, Andersen NH.** 2002. Designing a 20-residue protein. Nature structural biology **9:**425-430.

52. **Wise HM, Hutchinson EC, Jagger BW, Stuart AD, Kang ZH, Robb N, Schwartzman LM, Kash JC, Fodor E, Firth AE, Gog JR, Taubenberger JK, Digard P.** 2012. Identification of a novel splice variant form of the influenza A virus M2 ion channel with an antigenically distinct ectodomain. PLoS Pathog **8:**e1002998.

53. **Tong S, Li Y, Rivailler P, Conrardy C, Castillo DA, Chen LM, Recuenco S, Ellison JA, Davis CT, York IA, Turmelle AS, Moran D, Rogers S, Shi M, Tao Y, Weil MR, Tang K, Rowe LA, Sammons S, Xu X, Frace M, Lindblade KA, Cox NJ, Anderson LJ, Rupprecht CE, Donis RO.** 2012. A distinct lineage of influenza A virus from bats. Proceedings of the National Academy of Sciences of the United States of America **109:**4269-4274.

54. **Ye Z, Liu T, Offringa DP, McInnis J, Levandowski RA.** 1999. Association of influenza virus matrix protein with ribonucleoproteins. Journal of virology **73:**7467-7473.

55. **Bourmakina SV, Garcia-Sastre A.** 2003. Reverse genetics studies on the filamentous morphology of influenza A virus. The Journal of general virology **84:**517-527.

56. **Fu TM, Freed DC, Horton MS, Fan J, Citron MP, Joyce JG, Garsky VM, Casimiro DR, Zhao Q, Shiver JW, Liang X.** 2009. Characterizations of four monoclonal antibodies against M2 protein ectodomain of influenza A virus. Virology **385:**218-226.

57. **Lovell SC, Davis IW, Arendall WB, 3rd, de Bakker PI, Word JM, Prisant MG, Richardson JS, Richardson DC.** 2003. Structure validation by Calpha geometry: phi,psi and Cbeta deviation. Proteins **50:**437-450.

668
669
670

671 **FIGURE LEGENDS**

672

673 **FIG 1** Structure of M2e in complex with Fab65. (**A**) Left: Overall structure of the M2e
674 (magenta) and Fab65 (green for light chain and blue for heavy chain) complex. Upper right:
675 LCDR1 (dark green) flanks M2e (magenta), contacting the 3_{10}-helix. Lower right: Top view
676 with cartoon presentation of M2e (magenta) in complex with the heavy chain (marine) and
677 light chain (green) of Fab65. (**B**) Surface representation of M2e bound to Fab65 viewed from
678 the paratope towards M2e. M2e is color-coded according to the electrostatic potential. Color
679 scale was set from −10 kT/e (red) to 10 kT/e (blue), as calculated by the APBS tool plugged
680 in Pymol. LCDR and HCDR residues that interact with M2e are shown in stick presentation
681 in green and marine, respectively. (**C**) Comparison of shape complementarity scores of
682 different antibody-epitope complexes. Black bars represent shape complementarity (SC)
683 scores deduced from co-crystalized influenza hemagglutinin HA and Fab fragments
684 deposited in the PDB database. The red bar on the right indicates the SC of M2e/Fab65
685 (4N8C).

686 **FIG 2** Details of the main interactions between M2e and Fab65. (**A**) Close-up view of
687 hydrophilic interactions between M2e-Glu6 and Fab65. Dotted lines represent hydrogen
688 bonds and salt bridges. (**B**) Water mediated interactions and (**C**) other hydrophilic
689 interactions between M2e amino acid residues (colored in purple) and Fab65 amino acid
690 residues (light chain colored in green and heavy chain colored in blue). (**D**) Hydrophobic
691 interactions between M2e and mAb65 with surface presentation of Fab65 (left) and M2e
692 (right) color-coded according to the electrostatic potential. Colour scale was set from −10
693 kT/e (red) to 10 kT/e (blue), as calculated by the APBS tool plugged in Pymol. (**E**)
694 Reactivity of mAb65 and 14C2 with M2 was analyzed by western blot of lysates of HEK-

293T cells transfected with M2-Flag expression constructs carrying M2e-Ala mutants. Anti-Flag detection was used to normalize the amount of M2 in the cell lysates that were loaded. NC = negative control.

FIG 3 Binding of mAb65 to cells infected with influenza A virus. (**A**) Confocal images of immunofluorescence staining of MDCK cells infected with influenza virus. M2-staining is shown in red fluorescence and was revealed using mAb65 or mAb148 (TCN-031 like antibody, binds to the N-terminus of M2). Goat polyclonal antibody against influenza virus ribonucleoprotein (BEI Resources NR-3133) was used to stain viral RNPs (green). Cell nuclei were identified by DAPI staining (blue). (**B**) Amino acid sequence alignment of M2e from different influenza A viruses. The conserved Trp15 is highlighted in bold. (**C**) mAb65 does not affect influenza A virus plaque size. PR8, WSN, A/USSR/77 and X31 viruses were used in a plaque assay on MDCK cells in the presence of antibodies, amantadine or immune sera with virus neutralizing activity. The plaque assay was performed in a 96-well format and the plaques were visualised by immune-staining with goat anti-vRNP immune serum. mAb65, mAb148 and mAb3G8 (isotype matched negative control mAb) were used at a starting concentration of 10 µg/ml. Amantadine was used at a starting concentration of 100 µM. anti-HA means goat antiserum against PR8 virus (BEI Resources NR-3148) with strong neutralizing activity against PR8 and WSN viruses and some neutralizing activity against A/USSR/77 and X31 viruses. “Virus dilution” means serial tenfold dilution of the amount of virus that was used to inoculate the cells in the presence of mAb, amantadine or anti-HA serum, which were used as tenfold serial dilutions as indicated at the top.

FIG 4 Binding properties of mAb65 to M2e peptide and M2-expressing cells. (**A**) Binding of mAb65 and mAb148 to different M2e peptides. ELISA plates were coated with wild type

(WT), M2eW15G or M2eP10L M2e peptides at 20 ng/ml or 200 ng/ml as indicated. (**B**) Cellular ELISA using HEK-293T cells that had been transfected with wild type, M2Trp15Ala, or M2Pro10Ala M2-Flag expression vectors.

FIG 5 Structure of M2e. (**A**) Top: M2eTrp15 occupies a central position in M2e. The distance between the main chain oxygen of M2eLeu4 and the nitrogen of M2eGly16 is 3.1 Å (double arrow). Bottom: The β-turn involving Thr5 to Glu8 in M2e (left) and a 3_{10}-helix from Ile11 to Trp15 (right). Dotted lines represent hydrophilic interactions. (**B**) The position and interactions of M2eTrp15 in M2e (top) resemble those of Trp in a Trp-cage miniprotein (bottom). (**C**) Fourier transform infrared spectroscopy spectra of M2e peptides. Each spectrum was normalized and subtracted from the spectrum of the PBS buffer. Shown are FTIR spectra of wild-type M2e peptide (red), M2eW15G (blue) and M2eP10L (purple). The data shown are the average of 256 recorded spectra with a resolution of 2 nm.

FIG 6 Recombinant PR/8 virus with M2-Trp15 substitution is highly attenuated. Wild type PR/8 and PR/8 with M2 mutations that alter M2-Trp15 were generated by introducing the corresponding mutations in a plasmid-based reverse genetics system. Sets of eight plasmids were transfected into HEK293T-MDCK co-cultures to determine the expression of viral proteins and to try to rescue the virus. (**A**) Schematic representation of the codon usage and amino acid sequence near M2-Trp15 in M1 and M2 wild type and mutant PR/8 viruses (**B**) Western blot analysis of cell lysates prepared 24 h after transfection to evaluate expression of NP, M2 (revealed by staining with mAb148 and mAb65) and M1, as indicated. WT (wild type), NC (negative control, *i.e.* transfected with only pCAXL-PA, pCAXL-PB1, pCAXL-PB2, and pCAXL-NP), ST (Stop: mutant with stop codons introduced after M2-Asp24), NT (non-transfected). (**C**) Plaque assay to quantify rescued PR/8 viruses with introduced

741 M1/M2Trp15 mutations. (**D**) Hemagglutinating activity in the supernatant of transfected
742 HEK293T-MDCK co-cultures. The supernatant and serial three-fold dilutions were assayed
743 for hemagglutination of chicken red blood cells on day 2 or 5 after transfection with the
744 eight-plasmid system used for generating PR/8 virus.

745

746 **TABLE 1** Crystallographic X-ray diffraction and refinement statistics

Data statistics	**M2e peptide + Fab65**
Wavelength (Å)	0.980
Number of reflections (unique reflections)	429,800 (109,543)
Resolution range (Å)	50.0~1.60 (1.66~1.60)
Completeness (%)	96.9 (95.2)
R_{merge} (%)[a]	5.4 (67.4)
I/sigma	24.2 (1.8)
Space group	P1
Unit cell parameters (Å)	a=40.4, b=72.3, c=78.4
	α=86.9 °, β=77.5°, γ=84.6°
Refinement statistics	
Resolution range (Å)	38.4~1.6
Number of reflections	104,049
R/R_{free} (%)[b]	19.3/24.3
r.m.s. deviation	
bonds (Å)	0.019
angles (°)	1.96
# of water molecules	691
Average B (Å^2)	26.8
Ramachandran statistics (%)[c]	
Favored	97.5
Allowed	2.2
Outlier	0.1

747 [a]$R_{merge} = \Sigma|I - \langle I\rangle|/\Sigma\langle I\rangle$, where I and <I> are the measured and averaged intensities of
748 multiple measurements of the same reflection, respectively. The summation is over all the
749 observed reflections.

750 [b]$R = \Sigma|F_o - F_c|/\Sigma|F_o|$ calculated for all observed data. $R_{free} = \Sigma|F_o - F_c|/\Sigma|F_o|$ calculated for a
751 specified number of randomly chosen reflections that were excluded from the refinement.

752 [c]Calculated using RAMPAGE (57).

A

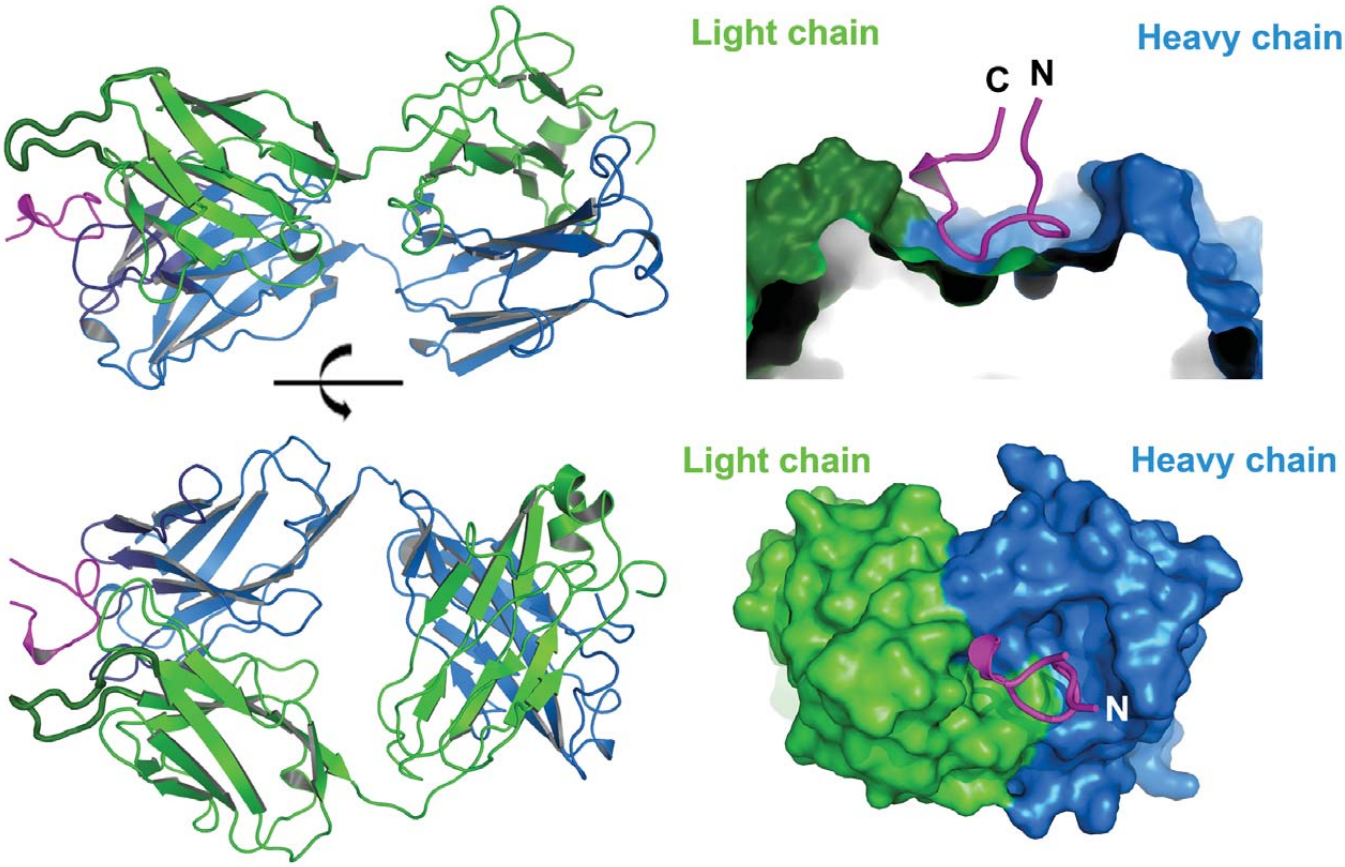

Fig. 1

B

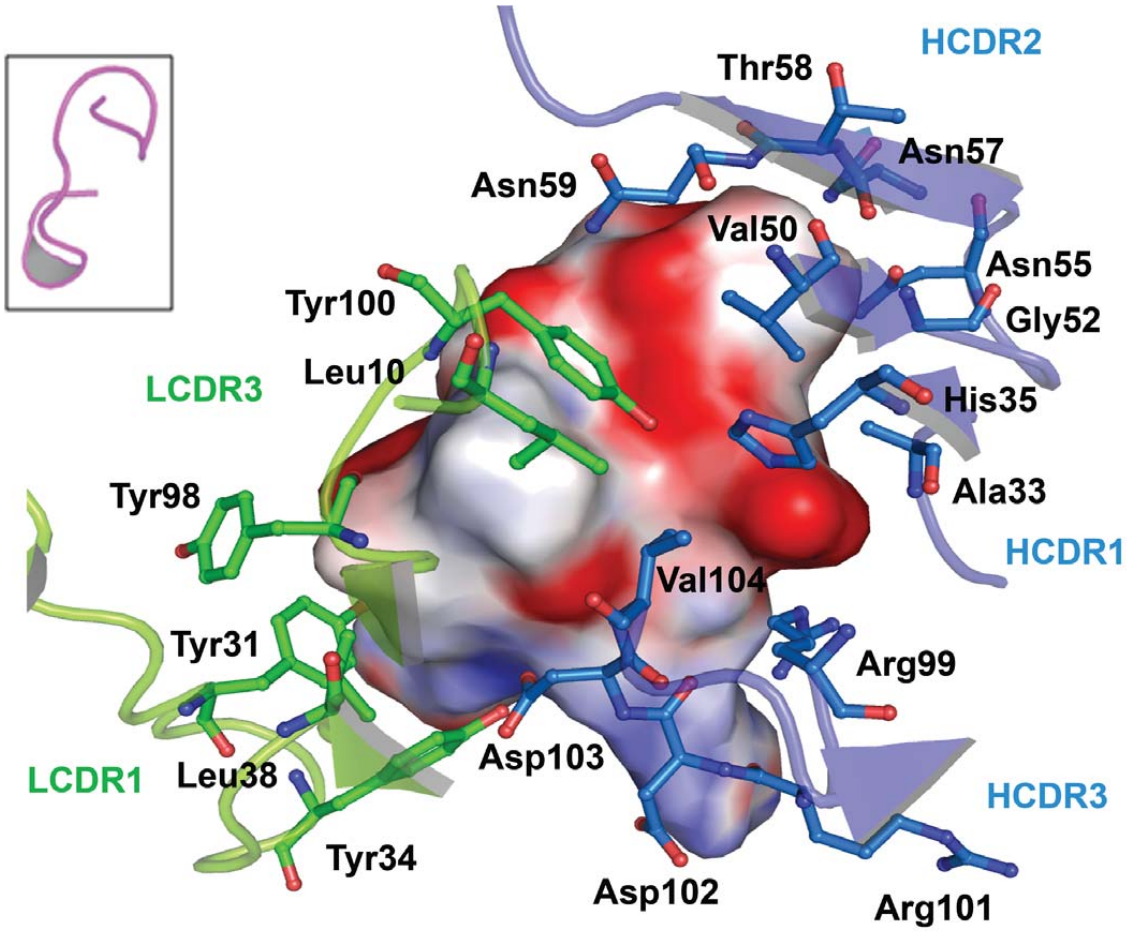

Fig. 1

C

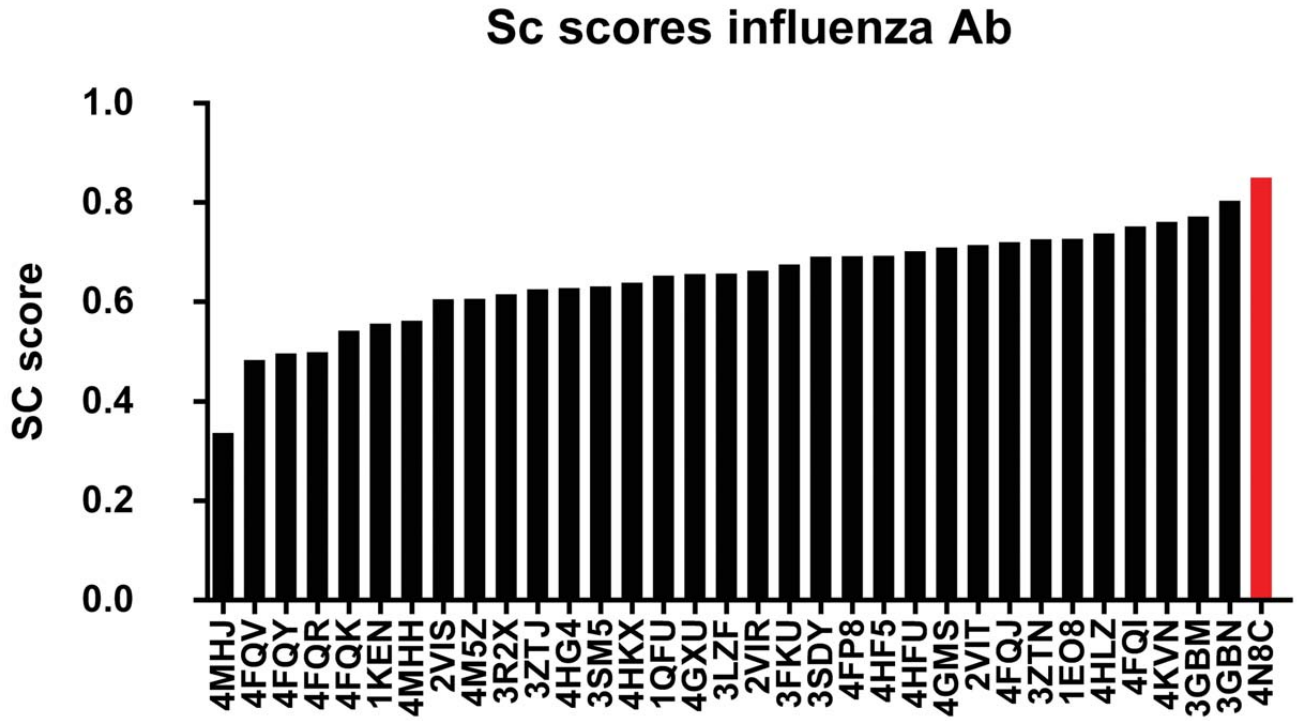

Fig. 1

A

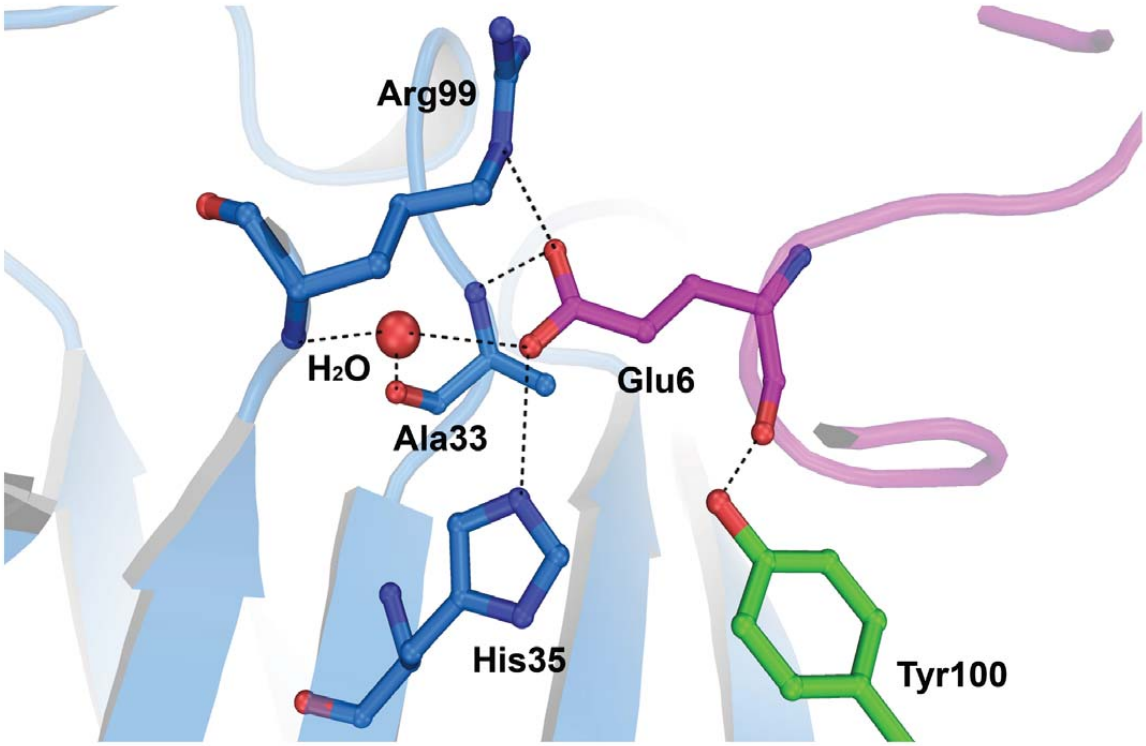

Fig. 2

B

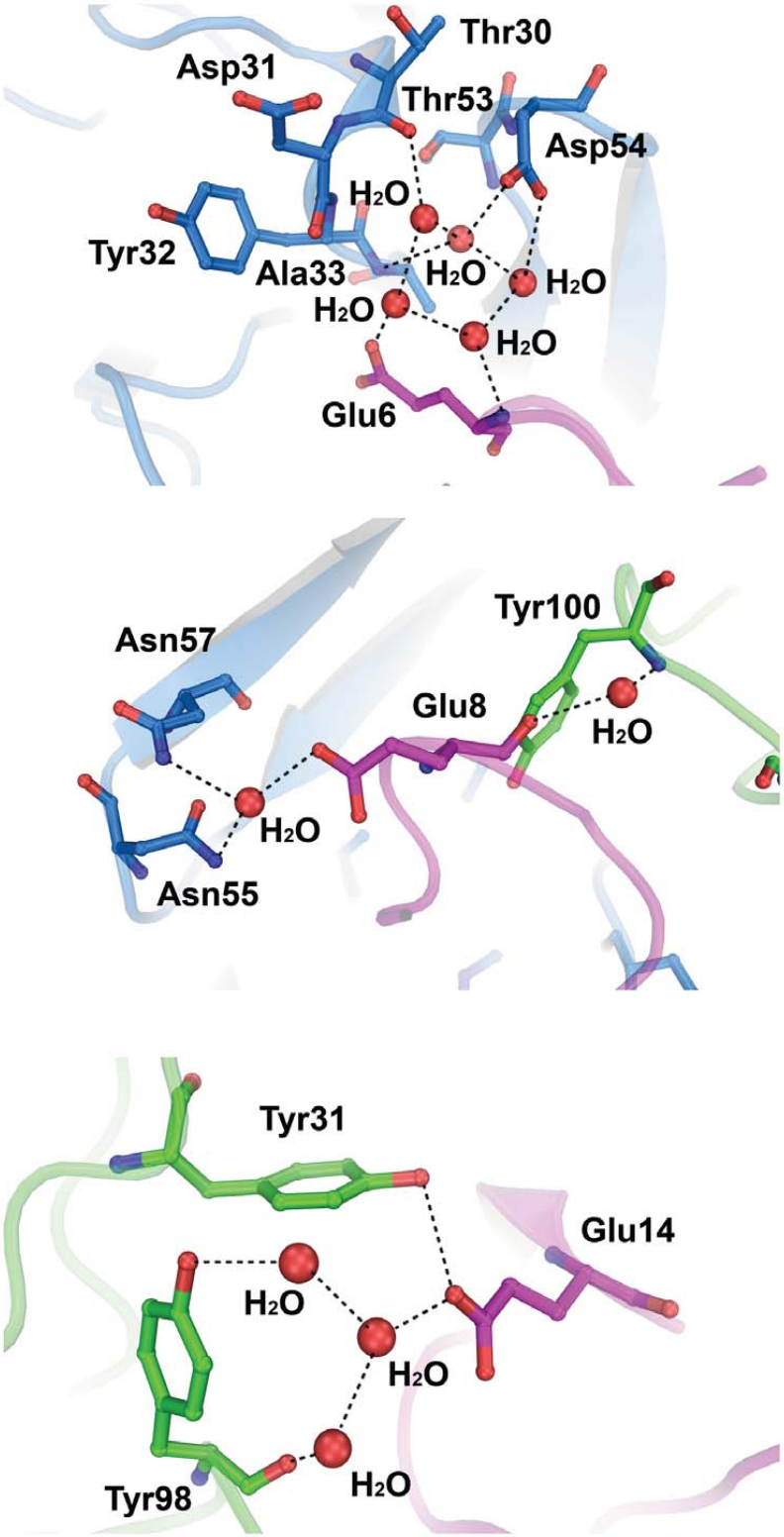

Fig. 2

C

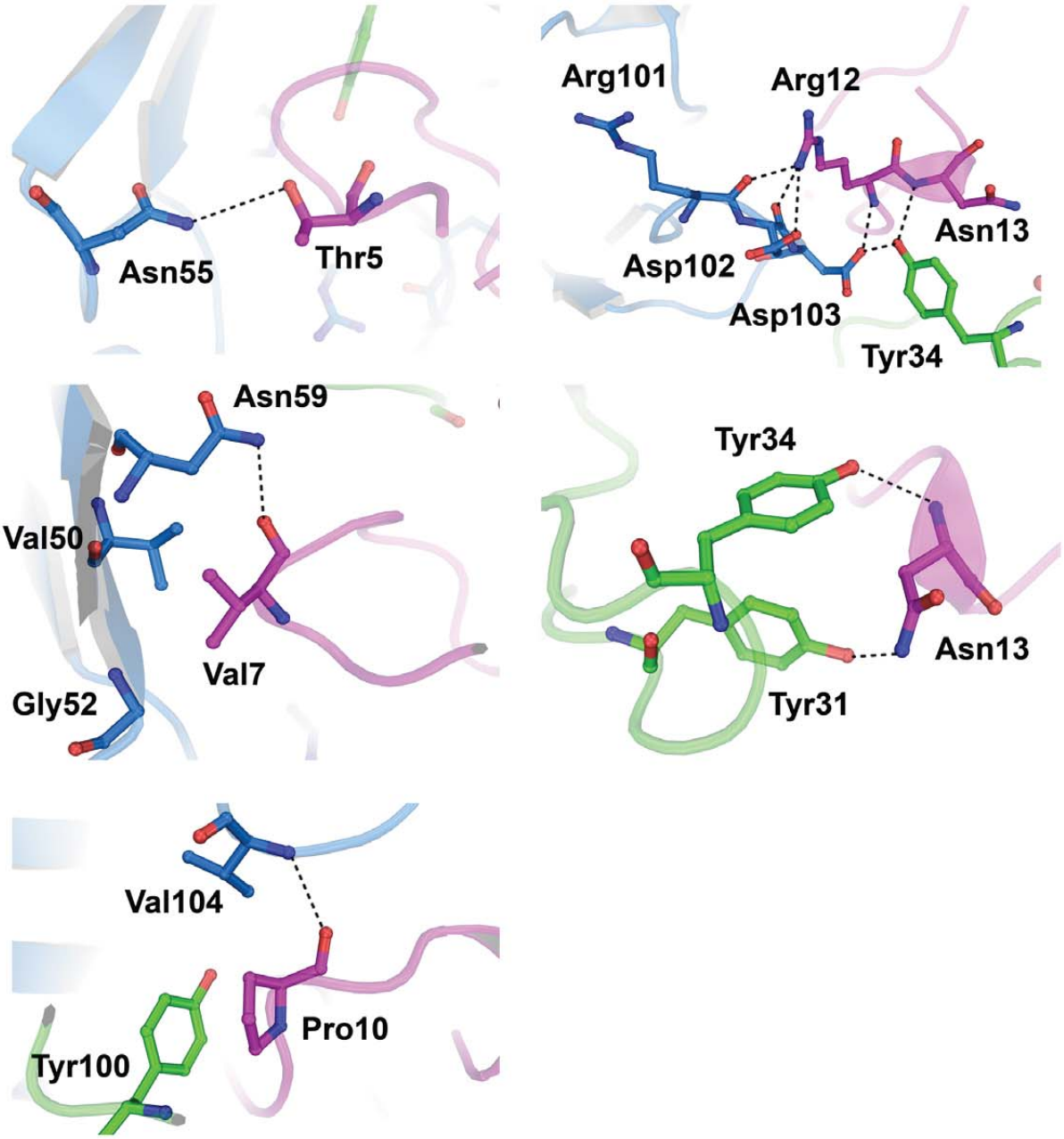

Fig. 2

D

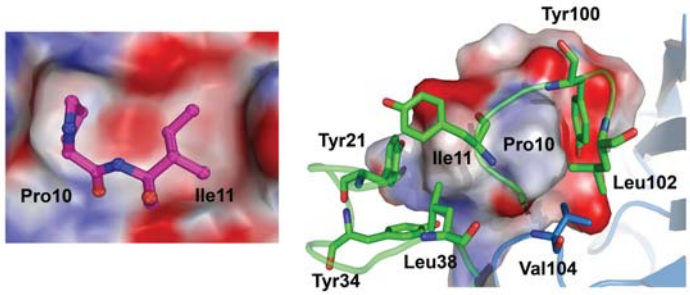

Fig. 2

E

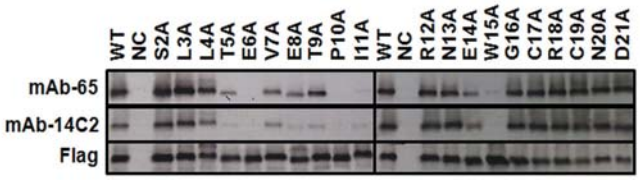

Fig. 2

A

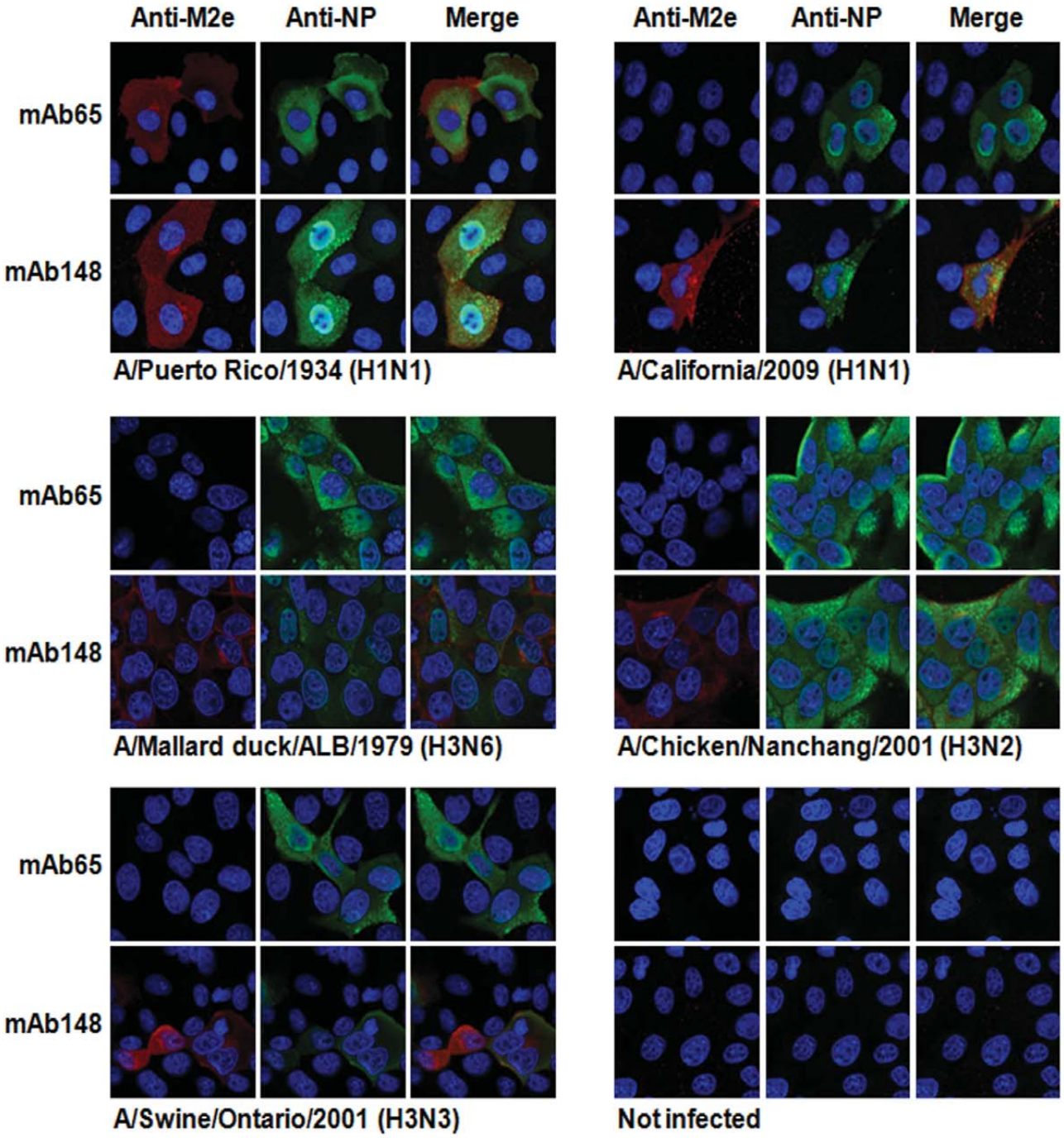

Fig. 3

B

```
A/Puerto Rico/8/1934 (H1N1)          : MSLLTEVETPIRNEWGCRCNDSSD
A/Brevig Mission/1/1918 (H1N1)       : ----------T-------------
A/California/07/2009 (H1N1)          : ----------T-S--E---S----
A/Mallard duck/ALB/676/1979 (H3N6)   : ---------LT--G-E-K-S----
A/Chicken/Nanchang/3-120/2001 (H3N2): ---------HT--G-----S----
A/Swine/Ontario/42729A/01 (H3N3)     : ----------T--G-E---S----
A/Vietnam/1203/2004 (H5N1)           : ----------T----E---S----
A/Shanghai/1/2013 (H7N9)             : ----------T-TG-E-N-SG--E
```

Fig. 3

C

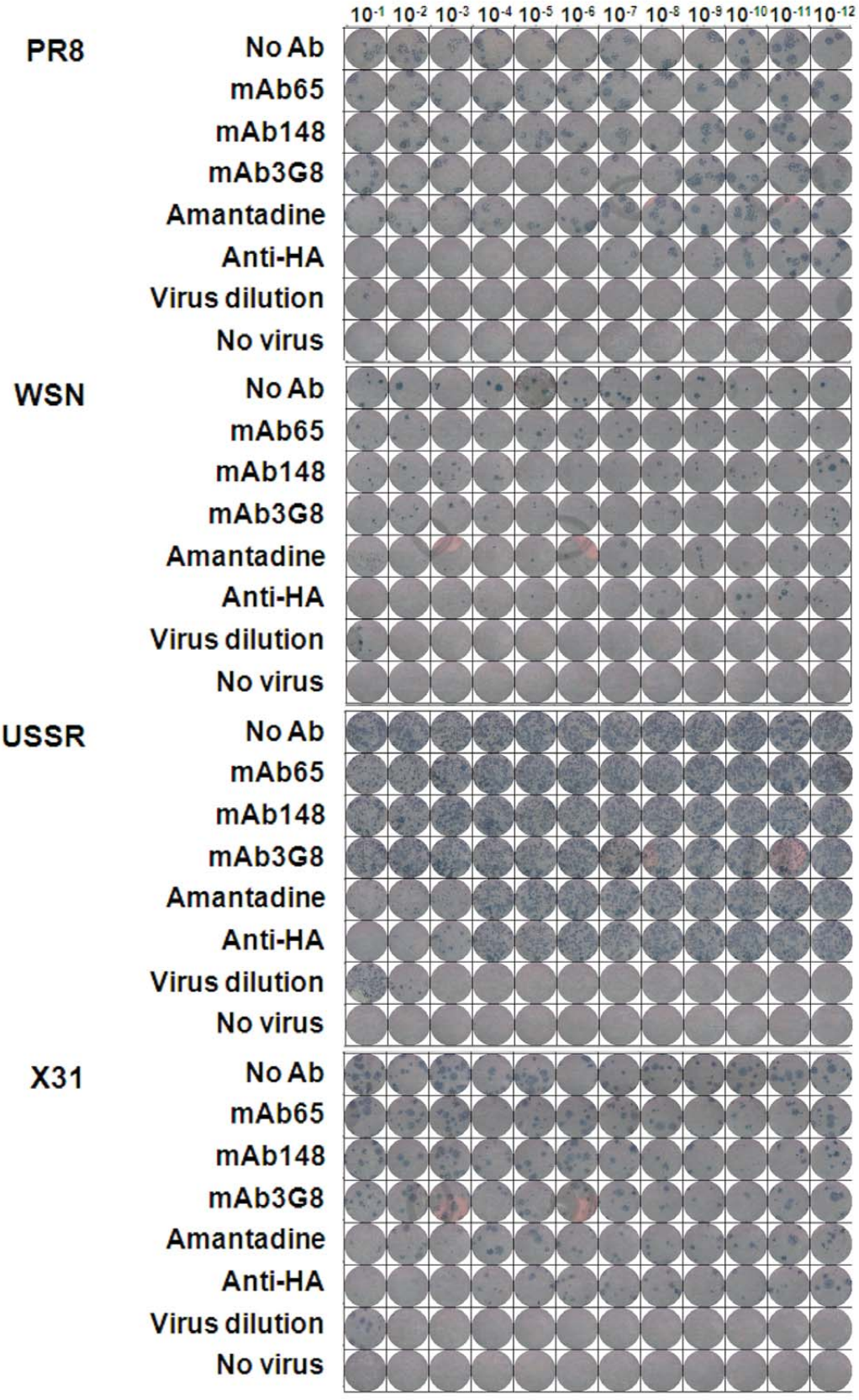

Fig. 3

A

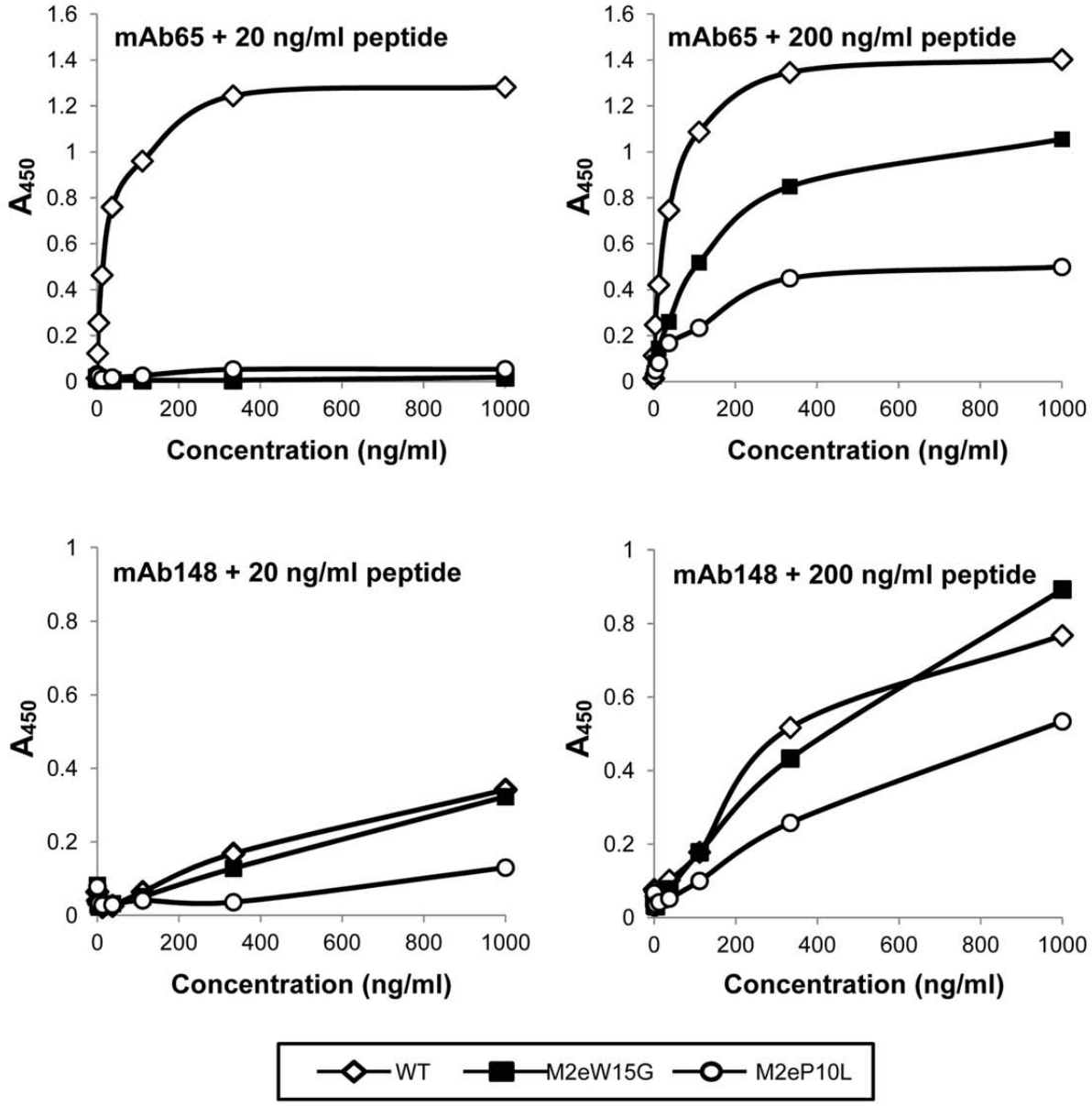

Fig. 4

B

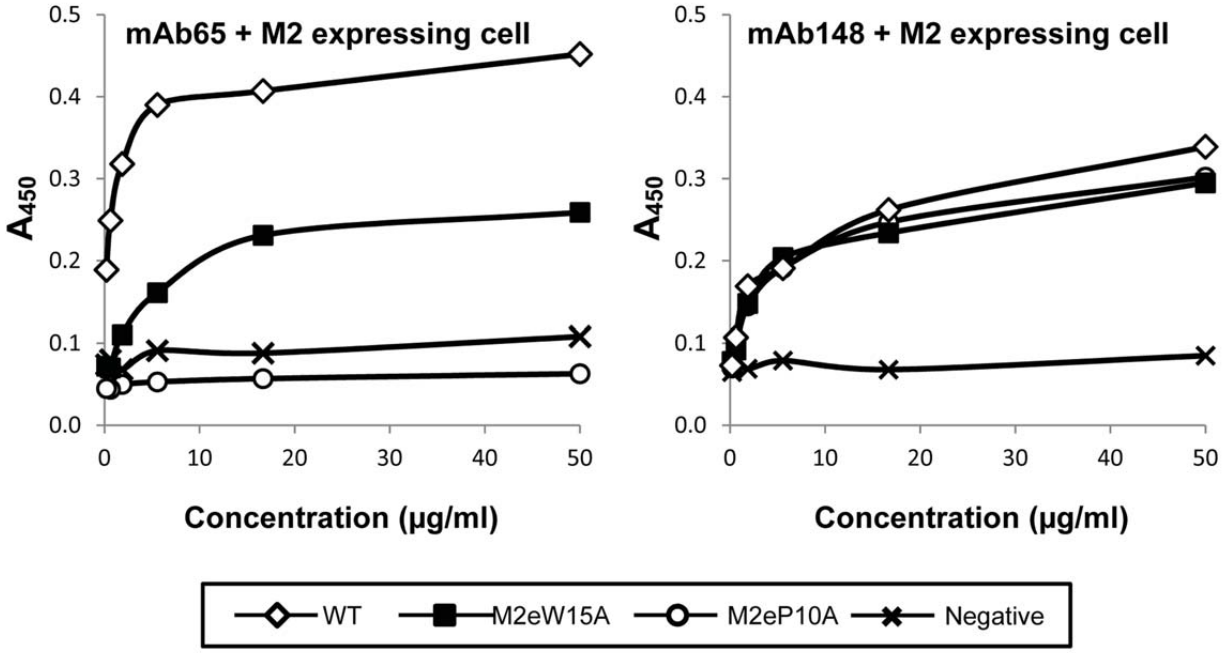

Fig. 4

A

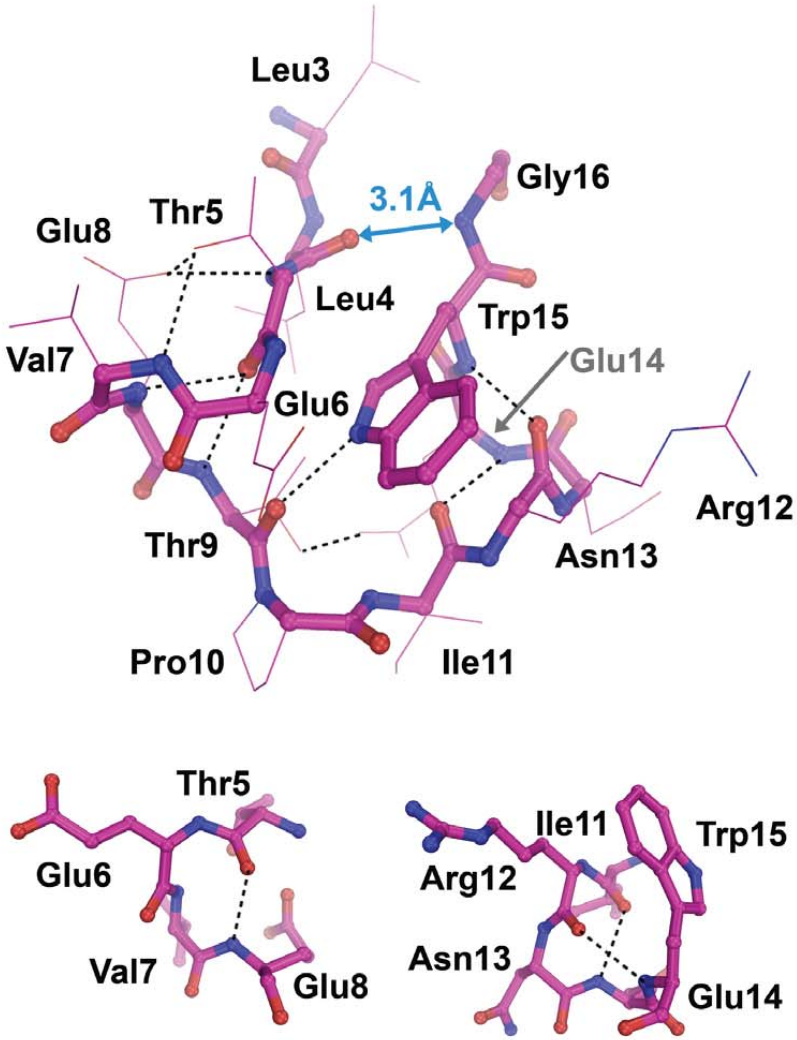

Fig. 5

B

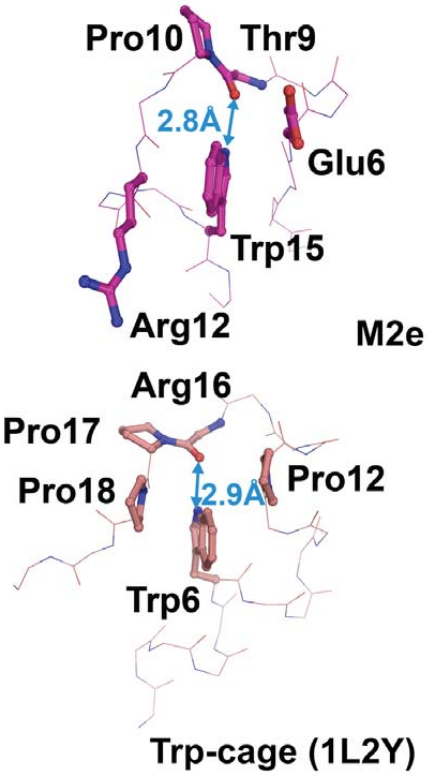

Fig. 5

c

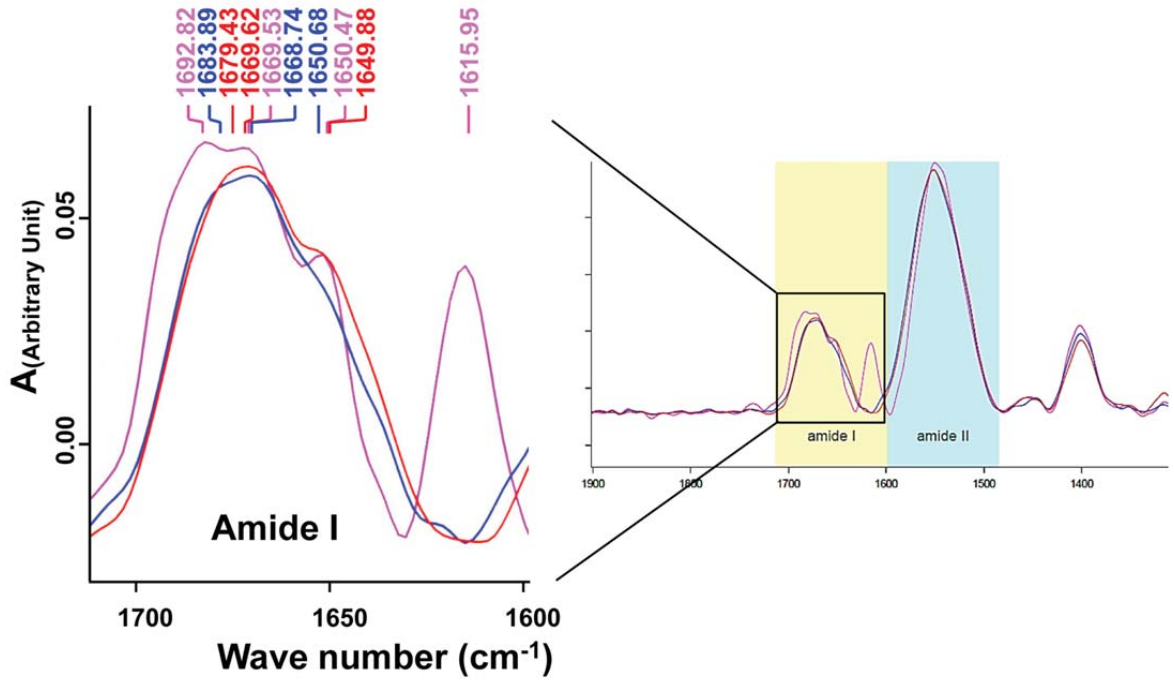

Fig. 5

A

Fig. 6

B

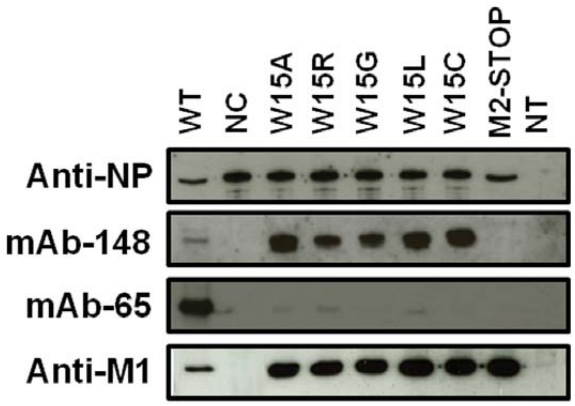

Fig. 6

C

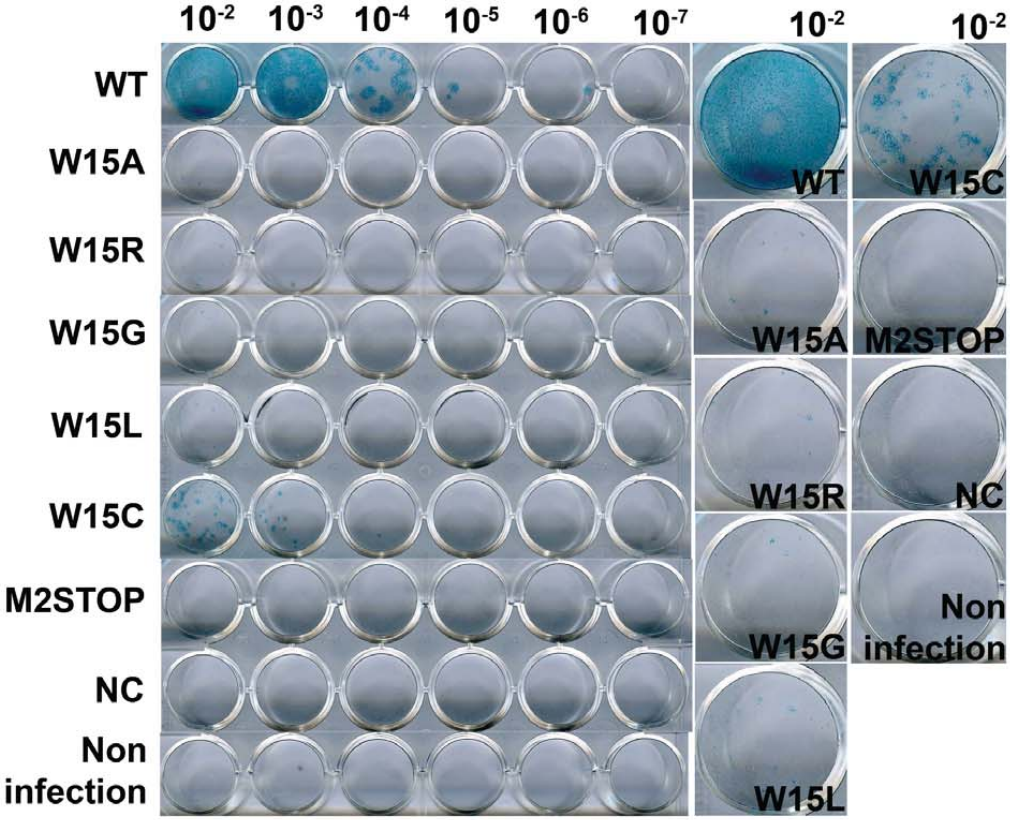

Fig. 6

D

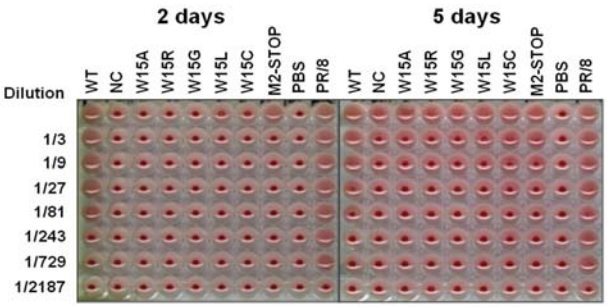

Fig. 6